ICES Journal of Marine Science

ICES Journal of Marine Science (2012), 69(7), 1194–1204. doi:10.1093/icesjms/fss111

Satellite remote sensing of primary productivity in the Bering and Chukchi Seas using an absorption-based approach

Toru Hirawake[1]*, Katsuhito Shinmyo[2], Amane Fujiwara[2], and Sei-ichi Saitoh[1]

[1]*Faculty of Fisheries Sciences, Hokkaido University, 3-1-1 Minato-cho, Hakodate, Hokkaido 040-8611, Japan*
[2]*Graduate School of Fisheries Sciences, Hokkaido University, 3-1-1 Minato-cho, Hakodate, Hokkaido 040-8611, Japan*

**Corresponding author: tel/fax: +81 138 408844; e-mail: hirawake@salmon.fish.hokudai.ac.jp.*

Hirawake, T., Shinmyo, K., Fujiwara, A., and Saitoh, S. 2012. Satellite remote sensing of primary productivity in the Bering and Chukchi Seas using an absorption-based approach. – ICES Journal of Marine Science, 69: 1194–1204.

Received 30 September 2011; accepted 14 May 2012.

Ocean colour remote sensing has been utilized for studying primary productivity in the Arctic Ocean. However, phytoplankton chlorophyll *a* (Chl *a*) is not predicted accurately because of the interference of coloured dissolved organic matter (CDOM) and non-algal particles (NAP). To enhance the estimation accuracy, a phytoplankton absorption-based primary productivity model (ABPM) was applied to the Bering and Chukchi Seas. The phytoplankton absorption coefficient was determined correctly from sea surface remote sensing reflectance (R_{rs}) and reduced the effect of CDOM and NAP in primary productivity (PP_{eu}) estimates. PP_{eu} retrieved from *in situ* R_{rs} using the ABPM satisfied a factor of 2 of measured values. PP_{eu} estimated from the Moderate Resolution Imaging Spectroradiometer R_{rs} data were within the range of historical values. These estimated PP_{eu} values were less than half of those of the model based on Chl *a*, and the difference between the two models reflected the influence of CDOM and NAP absorptions. Interannual variation in August and September over the period 2002–2010 showed an increase in primary productivity. The increase in 2007 was especially large, by a factor of 1.51–2.71, compared with 2006. The significant temporal increase in productivity detected here differs from earlier studies that detected little, if any, change in the region.

Keywords: absorption coefficient, Arctic Ocean, Bering Sea, Chukchi Sea, coloured dissolved organic matter (CDOM), ocean colour remote sensing, primary productivity.

Introduction

The continental shelves of the Chukchi and Bering Seas are some of the most productive ocean environments in the world. High primary production of phytoplankton in the region supports a large benthic biomass (Grebmeier *et al.*, 1988), providing food for organisms at higher trophic levels, such as fish, marine mammals, and seabirds (Moore *et al.*, 2003; Feder *et al.*, 2005). The high rate of primary productivity in the region is controlled by sea-ice cover, stratification by sea-ice melt water, and light conditions (Alexander and Niebauer, 1981), and is sustained with nutrients supplied from the warmer Pacific inflow (Grebmeier *et al.*, 2006a). Some abrupt changes in these controlling factors have appeared recently. The temperature of the Pacific summer water (Shimada *et al.*, 2006) and heat flux in the Bering Strait increased massively during the past decade (Mizobata *et al.*, 2010; Woodgate *et al.*, 2010), and it may accelerate sea-ice reduction in the Arctic Ocean. The sea-ice extent declined for 28 years from 1979 to 2006 (Parkinson and Cavalieri, 2008), especially during the Arctic winters of 2005 and 2006 (Comiso, 2006), and the minimum historical ice extent was in September 2007. Climate models predict that summer sea ice will disappear within this century (Boé *et al.*, 2009; Holland *et al.*, 2010). These environmental changes are expected to affect phytoplankton productivity and shift the Arctic ecosystem to one dominated by pelagic components (Piepenburg, 2005; Grebmeier *et al.*, 2006b). Knowledge of the spatio-temporal variability in primary productivity is important for predicting the impacts and responses of continental shelf ecosystems.

Satellite ocean colour remote sensing is a tool suitable for quantifying primary productivity in the ocean worldwide. Studies using satellite remote sensing have revealed an increase in annual primary production in the Arctic corresponding to the increase in open-water area (Arrigo *et al.*, 2008; Pabi *et al.*, 2008). However, there is an unresolved problem associated with the

detection of the subsurface chlorophyll maximum (SCM). Arrigo and van Dijken (2011) investigated the effect of the SCM on the estimation of annual primary production from satellite imagery, and they showed that neglecting the SCM results in a 7.6% underestimation of primary production.

Another uncertainty in the estimation of primary production is the accuracy of chlorophyll *a* (hereafter, Chl *a*) estimation used in algorithms. Coloured dissolved organic matter (CDOM) of terrestrial origin in the Arctic (Guéguen *et al.*, 2007) strongly affects the absorption of short wavelengths around 400 nm, which leads to an overestimation of Chl *a* concentration (Matsuoka *et al.*, 2007). It has great seasonality as a consequence of photobleaching and an additional injection of Alaskan Coastal Waters and creation of CDOM from the degradation of phytoplankton (Matsuoka *et al.*, 2011). Non-algal particles (NAP) and CDOM have similar effects on Chl *a* estimation and vary seasonally (Matsuoka *et al.*, 2011). More highly packaged pigments attributable to large cells such as diatoms also contribute to errors in Chl *a* estimation (Cota *et al.*, 2004). Matsuoka *et al.* (2007) demonstrated that the regionally tuned linear Chl *a* algorithm (Arctic OC4L) performs well in the western Arctic Ocean, but accurate retrieval of the photosynthetic rate has yet to be accomplished.

To reduce the uncertainty in Chl *a* estimation, an absorption-based primary productivity model (ABPM) was developed for the Southern Ocean (Hirawake *et al.*, 2011) as an improvement of the vertically generalized production model (VGPM; Behrenfeld and Falkowski, 1997). The ABPM uses the light absorption coefficient of phytoplankton, so it is possible to eliminate inputs of uncertain satellite Chl *a* data and photosynthetic rate as a function of satellite sea surface temperature (SST). If the phytoplankton absorption coefficient is retrieved from satellite data without the contamination of high CDOM and NAP absorptions, the ABPM is expected to present a more accurate estimation of primary productivity in the Arctic Ocean.

In this study, the phytoplankton absorption coefficient of discrete water samples was measured by the quantitative filter technique (QFT; Mitchell, 1990) and retrieved from *in situ* spectral radiation data using the quasi-analytical algorithm (QAA; Lee *et al.*, 2002, 2007b). These data were used to confirm the accuracy of the QAA estimation of the phytoplankton absorption coefficient after removal of CDOM and NAP contamination. The ABPM for the Chukchi and Bering Seas was developed based on an *in situ* dataset, and primary productivity was determined from the satellite-derived absorption coefficient of phytoplankton using the ABPM. Interannual variation in primary production over the shelf region was also assessed. Note that this method assumes that phytoplankton absorption from *in situ* and satellite spectral radiation data have the same relationship with absorption from the QFT.

Material and methods

Field surveys were carried out in the Bering Sea, Chukchi Sea, and Canada Basin during July/August 2007 (OS-180 cruise) and June/July 2008 (OS-190 cruise) aboard the TS "Oshoro-Maru", and during September/October 2009 (MR09-03 cruise) aboard the RV "Mirai" (Figure 1). At each station, measurements of spectral radiation, photosynthetically available radiation (PAR), and water was sampled for primary productivity, Chl *a* concentration, and light absorption coefficient. Seawater samples were collected from the sea surface and several depths corresponding to light levels at 50, 25, 10, 5, and 1% of incident PAR using Niskin bottles on a Carousel water sampler equipped with a CTD (Sea-Bird Electronics, Inc.). The light levels of PAR in water were determined using a PAR sensor (LI-193SA, LI-COR) or underwater spectroradiometers. The total number of sampling stations was 42.

Chl *a* concentration

Chl *a* concentration was determined with both fluorometry and high-performance liquid chromatography (HPLC) for the OS-180 and MR09-03 cruises, and with fluorometry only for the OS-190 cruise.

A 200 ml sample of seawater was filtered onto a glassfibre filter (Whatman GF/F, 25 mm diameter) for fluorometric determination. The filter was immediately soaked in *N*,*N*-dimethylformamide (DMF), and pigments were extracted for 24 h in the dark at −20°C (Suzuki and Ishimaru, 1990). The fluorescent intensity was measured with a Turner Designs 10AU fluorometer calibrated against a pure Chl *a* standard (Sigma), and Chl *a* concentration was calculated according to the non-acidification method (Welschmeyer, 1994).

For HPLC analysis, a few litres of seawater were passed through 20- and 5-μm nylon mesh filters and GF/F filters (Whatman 47 mm diameter) during the OS-180 cruise, and filtered onto a 25 mm Whatman GF/F filter for the MR09-03 cruise under gentle vacuum pressure (<100 mmHg). The filter samples were stored in liquid nitrogen in a deep-freezer (−80°C). Phytoplankton pigments were extracted with DMF (Suzuki *et al.*, 2005) and analysed with HPLC according to the methods in Suzuki *et al.* (2005; OS-180 cruise) and van Heukelem and Thomas (2001; MR09-03 cruise) to determine Chl *a* concentration. For the OS-180 cruise, a summation of Chl *a* concentration for three filter types (20 and 5 μm and GF/F) was calculated.

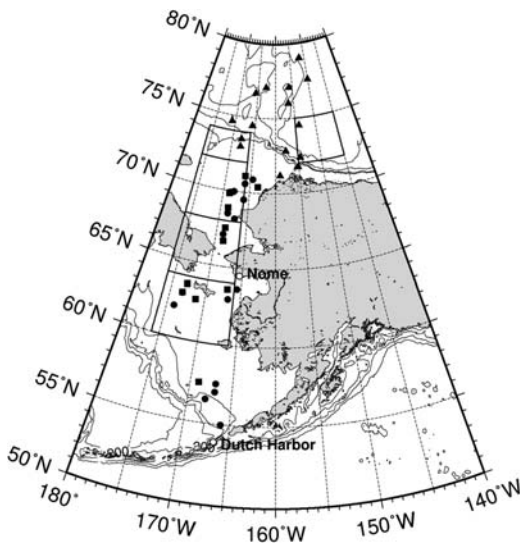

Figure 1. Map of the sampling stations. Circles, squares, and triangles are sampling locations during the OS-180, OS-190, and MR09-03 cruises, respectively, and cells surrounded by thick lines show the regions from which interannual variation in primary productivity was extracted, from south to north, the northern Bering Sea, the Bering Strait, the Chukchi shelf, the shelf break, and the Canada Basin.

Primary productivity

Samples were transferred into 500 or 1000 ml acid-cleaned clear polycarbonate bottles, and their light intensity exposure was regulated to corresponding depths with black neutral-density mesh. After adding $NaH^{13}CO_3$ (99 atom% ^{13}C, Shoko Co. Ltd) solution with ~10% of total carbonate, the samples were incubated under natural incident light for 24 h in a water bath on deck. Temperature in the water bath was maintained with running water pumped from the sea surface. Daily sea surface PAR, E_0, was monitored with a LI-190SB air quantum sensor (LI-COR) and recorded into a LI-1400 data logger (LI-COR). After incubation, the water sample was filtered onto a pre-combusted glassfibre filter (Whatman GF/F, 25 mm diameter) under gentle vacuum pressure (<100 mmHg). The filter samples were frozen in liquid nitrogen and stored in a deep-freezer until analysed. The stored filters were thawed and exposed to fumes of hydrochloric acid, to remove inorganic carbon. Particulate organic carbon and the isotope ratios (^{12}C and ^{13}C) of the samples were determined using an isotope ratio mass spectrometer (DELTA^{Plus} ADVANTAGE, Thermo Finnigan) and an in-line elemental analyser (Flash EA 1112, Thermo Finnigan), or an isotope ratio mass spectrometer with an on-line elemental analyser (ANCA-NT, Europa Scientific). Daily net primary productivity at depth z, $P(z)$, was calculated from the isotope ratio using the equation of Hama *et al.* (1983). Water column daily primary productivity PP_{eu} was calculated as follows:

$$PP_{eu} = \int_0^{Z_{eu}} P(z)\,dz, \tag{1}$$

where Z_{eu} is the euphotic zone depth (a depth of 1% PAR). The photosynthetic rate at depth z, $P^B(z)$, is defined as

$$P^B(z) = \frac{P(z)}{C(z) \times D_{irr}}, \tag{2}$$

where $C(z)$ is the Chl *a* at depth z, and D_{irr} the photoperiod. The maximum value of $P^B(z)$ in the water column is P^B_{opt} (Behrenfeld and Falkowski, 1997).

Spectral radiation

Underwater downward spectral irradiance, $E_d(\lambda, z)$, and upward spectral radiance, $L_u(\lambda, z)$, were measured with a HyperPro (Satlantic Inc.) for the OS-180 and OS-190 cruises, or a PRR-800 spectroradiometer (Biospherical Instruments Inc.) for the MR09-03 cruise. Although the HyperPro measures radiation at 136 wavelengths between 350 and 800 nm, the PRR-800 has 17 wavelengths between 380 and 765 nm. Both instruments are the freefall type intended to be deployed away from the ship, to minimize shadow effects. PAR was calculated at each depth to determine the sampling depths, integrating $E_d(\lambda, z)$ over wavelength λ from 400 to 700 nm. Incident irradiance at the sea surface, $E_{ds}(\lambda, z)$, was also monitored by reference spectroradiometers with the same specifications as the underwater sensor and used for correction and the radiometric calculations described below.

To investigate the retrieval accuracy of the absorption coefficient from radiation data, the remote sensing reflectance, R_{rs}, was calculated from the *in situ* spectral radiation data. Values of $E_d(\lambda, z)$ and $L_u(\lambda, z)$ at just below the sea surface, $E_d(\lambda, 0-)$ and $L_u(\lambda, 0-)$, were defined by extrapolating the data between 2–3 and 10 m to just below the sea surface ($z = 0-$) according to the following equations (Gordon *et al.*, 1983):

$$E_d(\lambda, z) = E_d(\lambda, 0-) \times \exp[-K_d(\lambda) \times z], \tag{3}$$

and

$$L_u(\lambda, z) = L_u(\lambda, 0-) \times \exp[-K_u(\lambda) \times z], \tag{4}$$

where λ is the wavelength, z the depth, K_d the diffuse attenuation coefficient of downward irradiance, and K_u the diffuse attenuation coefficient of upward radiance. Water leaving radiance (Austin, 1974), $L_w(\lambda)$, was calculated from

$$L_w(\lambda) = \left(\frac{t}{n^2}\right) \times L_u(\lambda, 0-), \tag{5}$$

where t is the surface transmittance from sea to air, and n the refractive index of seawater. Parameters t and n are ~0.98 and 1.341 (Austin, 1974), respectively. The normalized water-leaving radiance, $L_{wn}(\lambda)$, is defined as follows:

$$L_{wn}(\lambda) = L_w(\lambda) \times \frac{\bar{F}_o(\lambda)}{E_{ds}(\lambda)}, \tag{6}$$

where $\bar{F}_o(\lambda)$ is the mean extraterrestrial solar irradiance (Neckel and Labs, 1984), and $E_{ds}(\lambda)$ the incident irradiance at the sea surface. Finally, the remote sensing reflectance, $R_{rs}(\lambda)$, can be expressed by the equation

$$R_{rs}(\lambda) = \frac{L_w(\lambda)}{E_{ds}(\lambda)}. \tag{7}$$

Absorption coefficient

Particles in the seawater sample were concentrated on a glassfibre filter (Whatman GF/F, 25 mm). The optical density (OD) of particles on the filter pad was measured with a spectrophotometer, MPS-2400 or MPS-2450 (Shimadzu). Both these spectrophotometers are equipped with a diffuser and a light guide tube between the sample and an end-on type photomultiplier, to minimize the loss of scattered light. The absorption coefficient of particles, $a_p(\lambda, z)$, was determined from the OD according to the QFT (Mitchell, 1990). The filter was replaced on the filtration system, then soaked in methanol to remove the pigments (Kishino *et al.*, 1985), the OD was measured again, and the absorption coefficient of NAP, $a_d(\lambda, z)$, was determined. The absorption coefficient of phytoplankton, $a_{ph}(\lambda, z)$, was calculated by subtracting $a_d(\lambda, z)$ from $a_p(\lambda, z)$.

For the sea surface $a_{ph}(\lambda, 0-)$ measured by QFT, the spectrally averaged absorption coefficient, $\bar{a}_{ph}(0-)$, was determined by assuming a flat (constant over the visible region) $E_d(\lambda, 0-)$ spectrum in quantum units (Hirawake *et al.*, 2011):

$$\bar{a}_{ph}(0-) = \frac{\int_{400}^{700} a_{ph}(\lambda, 0-)\,d\lambda}{700 - 400} \tag{8}$$

To derive $\bar{a}_{ph}(0-)$ from the Moderate Resolution Imaging Spectroradiometer (MODIS) data, the empirical relationship between $\bar{a}_{ph}(0-)$ from Equation (8) and the approximate value by trapezoidal integration of $a_{ph}(\lambda, 0-)$ at the wavelengths of MODIS bands (412–555 nm) was prepared using *in situ* data [shown in Equation (11)].

The QAA (Lee *et al.*, 2002, 2007b) was applied to estimate both $a_{ph}(\lambda, 0-)$ and the summation of absorption coefficients by CDOM and NAP, $a_{dg}(\lambda, 0-)$, from *in situ* and MODIS $R_{rs}(\lambda)$. $R_{rs}(\lambda)$ can be expressed as a function of the absorption coefficient and the backscattering coefficient (Gordon *et al.*, 1988). The QAA inversely calculates the total absorption coefficient and backscattering coefficient of particles from $R_{rs}(\lambda)$ at several wavelengths, then decomposes the total absorption coefficient to $a_{ph}(\lambda)$ and $a_{dg}(\lambda)$ using empirical, semianalytical, and analytical approaches.

Primary productivity model

The VGPM is a function of satellite-derived Chl *a* and SST (Behrenfeld and Falkowski, 1997):

$$PP_{eu} = P^{B}_{opt} \times \frac{0.66125 \times E_0}{E_0 + 4.1} \times Z_{eu} \times C_{surf} \times D_{irr} \quad (9.1)$$

where C_{surf} is sea surface Chl *a* concentration. Behrenfeld and Falkowski (1997) used the seventh-order polynomial function of SST to derive P^{B}_{opt}. Marra *et al.* (2007) showed that light-saturated or near-surface primary productivity has a linear and invariant relationship with a phytoplankton absorption coefficient such as $\bar{a}_{ph}(0-)$, not a Chl *a*-specific absorption coefficient, rather than with Chl *a* concentration in the world ocean. They also suggested that environmental variability is expressed through the absorption properties of phytoplankton. The surface primary productivity in Marra *et al.* (2007) corresponds to the term $P^{B}_{opt} \times C_{surf}$ in Equation (9.1). Moreover, information on the Chl *a* biomass is included in the phytoplankton absorption coefficient (Hirawake *et al.*, 2011). Therefore, $P^{B}_{opt} \times C_{surf}$ was replaced by an empirical function of $\bar{a}_{ph}(0-)$. In this study, $a_{ph}(443, 0-)$ was also used to replace $P^{B}_{opt} \times C_{surf}$. Note that a homogeneous distribution of vertical Chl *a* concentration is assumed, and its concentration is the same as the C_{surf} in the context of this model. Consequently, the ABPM is as follows:

$$PP_{eu} = f\,[\bar{a}_{ph}(0-)] \times \frac{0.66125 \times E_0}{E_0 + 4.1} \times Z_{eu} \times D_{irr} \quad (9.2)$$

or

$$PP_{eu} = f\,[a_{ph}(443, 0-)] \times \frac{0.66125 \times E_0}{E_0 + 4.1} \times Z_{eu} \times D_{irr} \quad (9.3)$$

Satellite data

Two methods for PP_{eu} estimation, VGPM and ABPM, were compared using the latest reprocessing version (2010.0) of Aqua MODIS Level 3 standard mapped images (SMI; monthly and daily 4 km resolution) for the years 2002–2010. PP_{eu} was derived from the VGPM using the SMI of Chl *a* concentration (C_{surf}), SST, PAR (E_0), and Z_{eu} from Morel's algorithm (Morel and Maritorena, 2001), and from the ABPM using the SMI of $a_{ph}(443)$ and Z_{eu} from the QAA (Lee *et al.*, 2002, 2007b). Daily images within ± 2 d of the dates of *in situ* measurements were used to validate PP_{eu}.

The MODIS data in 2009 and 2010 had an inconsistent value of R_{rs} at 412 and 443 nm. Reprocessing to improve these values was carried out in 2011 (the details are described in http://oceancolor.gsfc.nasa.gov/WIKI/OCReproc20100MA.html), and the data used in this study are the corrected data.

Performance of model

The performance of the models used to estimate absorption coefficients and primary productivity were evaluated using the root-mean square of log-difference error (RMSE) (Campbell *et al.*, 2002), defined as

$$\mathrm{RMSE} = \sqrt{\frac{1}{N}\sum_{i=1}^{N}(\log_{10}\mathrm{Mod}_i - \log_{10}\mathrm{Meas}_i)^2} \quad (10)$$

where N is the number of data, and Mod and Meas are modelled and measured values, respectively. RMSE values <0.3 indicate agreement of modelled and measured values within a factor of 2 (Hill and Zimmerman, 2010).

Results

In situ daily primary productivity

In situ column-integrated daily primary productivity in this study ranged from 13 to 1414 mg C m^{-2} d^{-1} (Table 1). The lowest and highest values were found at stations in the Canada Basin and the Bering Strait, respectively. September productivity in the Canada Basin was consistently low, and its mean value was 25 mg C m^{-2} d^{-1} with a range of 13–46 mg C m^{-2} d^{-1}. Productivity data with phytoplankton absorption data from all stations of all areas ($n = 42$) were used for model development.

Absorption coefficient derivation

The estimation accuracy of the absorption coefficient of phytoplankton using the remote sensing reflectance $R_{rs}(\lambda)$ was confirmed before the construction of a primary productivity model, because of the possible effect of high CDOM and NAP absorptions in the study area. Although the spectrally averaged absorption coefficient, $\bar{a}_{ph}(0-)$, expressed by Equation (8) uses values over whole visible wavelengths, the MODIS has a limited number of

Table 1. *In situ* daily primary productivity for each study area.

			Primary productivity (mg C m^{-2} d^{-1})		
Area	**Month and year**	***n***	**Mean**	**Minimum**	**Maximum**
Canada Basin	September–October 2009	10	25	13	46
Shelf break	September–October 2009	4	53	38	74
Chukchi shelf	August 2007, July 2008, October 2009	12	286	36	642
Bering Strait	August 2007, July 2008	3	704	114	1 414
Northern Bering Sea	July–August 2007, July 2008	8	191	70	301
Southern Bering Sea	July 2007, June 2008	5	388	153	1 015
All areas		42	225	13	1 414

spectral bands, and reflectance at longer wavelengths is generally weak. Therefore, the following empirical relationship between $\bar{a}_{ph}(0-)$ and the integrated value of $a_{ph}(\lambda, 0-)$ at the wavelengths of MODIS bands from 412 to 555 nm was established using *in situ* data measured by the QFT:

$$\bar{a}_{ph}(0-) = \frac{1.5354 \times \sum_{i=1}^{4} [(a_{ph}(\lambda_{i+1}) + a_{ph}(\lambda_i)) \times (\lambda_{i+1} - \lambda_i)/2]}{700 - 400} \quad (11)$$

($r^2 = 0.992$, $n = 42$, $p < 0.001$), where wavelengths from λ_1 to λ_5 are 412, 443, 488, 531, and 555 nm, respectively. The value of the integration part of the numerator in Equation (11) derived from $R_{rs}(\lambda)$ using the QAA was compared with the measured value from the QFT (Figure 2a). $R_{rs}(\lambda)$ calculated from *in situ* spectral radiation measured with spectroradiometers according to Equations (3)–(7) was used for the comparison, because there were insufficient satellite matchup data to evaluate the validation result attributable to cloud cover. Most of the integrated $a_{ph}(412–555)$ values using QAA estimation coincided with the measured QFT value within a factor of 2, and half the data satisfy a factor of 1.5 accuracy. However, underestimation of integrated $a_{ph}(412–555)$ leads to a slightly high RMSE (0.353). Further, negative values of $a_{ph}(412)$ were frequently found in the MODIS images when the absorption was low, probably because of atmospheric correction or a limitation of the current version of QAA. Alternatively, utilization of only $a_{ph}(443)$, which is a peak of Chl *a* absorption, was tested to reduce missing values attributed to this error in primary productivity calculations from satellite data. Estimated $a_{ph}(443)$ using the QAA also exhibited better agreement (RMSE = 0.250) with the measured $a_{ph}(443)$ from the QFT. Overall, 86 and 69% of data were within a factor of 2 and 1.5, respectively (Figure 2b). Therefore, $a_{ph}(443)$ was more accurate for the analysis using the QAA in this study and maximized the availability of MODIS data.

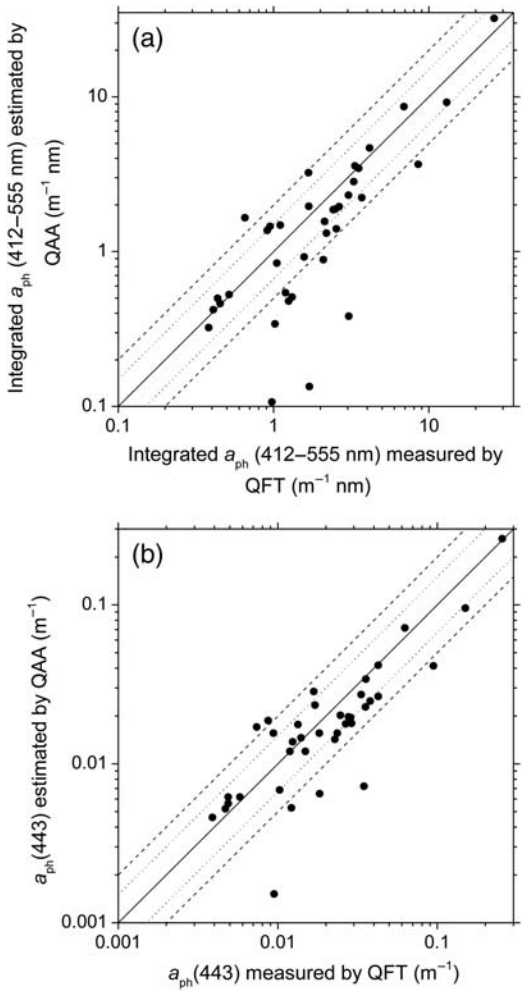

Figure 2. Comparison of absorption coefficients between measured (QFT data) and estimated (*in situ* spectroradiometer data input into the QAA) values. (a) Integrated value of a_{ph} using five MODIS bands from 412 to 555 nm. (b) a_{ph} at 443 nm. The solid line represents 1:1 agreement, and dashed and dotted lines represent factors of 2 and 1.5 relative errors.

Estimation of primary productivity

A key modification of the ABPM in this study is the substitution of the light-absorption coefficient of phytoplankton [Equations (9.2) and (9.3)] for the product of P^B_{opt} and C_{surf} in the VGPM [Equation (9.1)]. To use the absorption model, a regular relationship between these two values is required, as in the case of the Southern Ocean, where a simple linear regression was applied (Hirawake *et al.*, 2011). The relationships between $P^B_{opt} \times C_{surf}$ and sea surface absorption coefficients $\bar{a}_{ph}(0-)$ and $a_{ph}(443, 0-)$ from measured QFT data are plotted in Figure 3a and b, respectively. The $P^B_{opt} \times C_{surf}$ significantly ($p < 0.001$) increased in proportion to both absorption coefficients, and power functions were a better fit than linear expression for these relationships:

$$P^B_{opt} \times C_{surf} = 266.54 \times \bar{a}_{ph}(0-)^{1.366} (r^2 = 0.806, n = 42), \quad (12)$$

and

$$P^B_{opt} \times C_{surf} = 102.44 \times a_{ph}(443, 0-)^{1.431} (r^2 = 0.795, n = 42). \quad (13)$$

Although Equation (12) gives a better result than Equation (13), the latter using $a_{ph}(443, 0-)$ was applied to the MODIS data in this paper to minimize missing values attributed to a negative value of $a_{ph}(412)$. The relationship using $\bar{a}_{ph}(0-)$, i.e. Figure 3a and Equation (12), is for use when the correct estimation of $a_{ph}(412, 0-)$ from satellite imagery is available. The $a_{ph}(443, 0-)$ value retrieved from $R_{rs}(\lambda)$ data from the *in situ* spectroradiometer and MODIS was tuned to the measured value as closely as possible, using the relationship in Figure 2b to reduce the bias of the QAA algorithm.

The ABPM using $a_{ph}(443, 0-)$ satisfies the factor of 2 in accuracy (RMSE = 0.268) when the $a_{ph}(443, 0-)$ and Z_{eu} values in Equation (9.3) are estimated from *in situ* $R_{rs}(\lambda)$ using the QAA (Figure 4). On the other hand, a few estimations near the coast and sea-ice edge using the MODIS $R_{rs}(\lambda)$ values were clearly overestimated around 60–70 mg C m^{-2} d^{-1}. Because the MODIS data were not available for the same day as the *in situ* measurements, the date for matchup was extended to ±2 d. The overestimation could probably be attributed to large and fast fluctuations of coastal waters and the movement of sea ice.

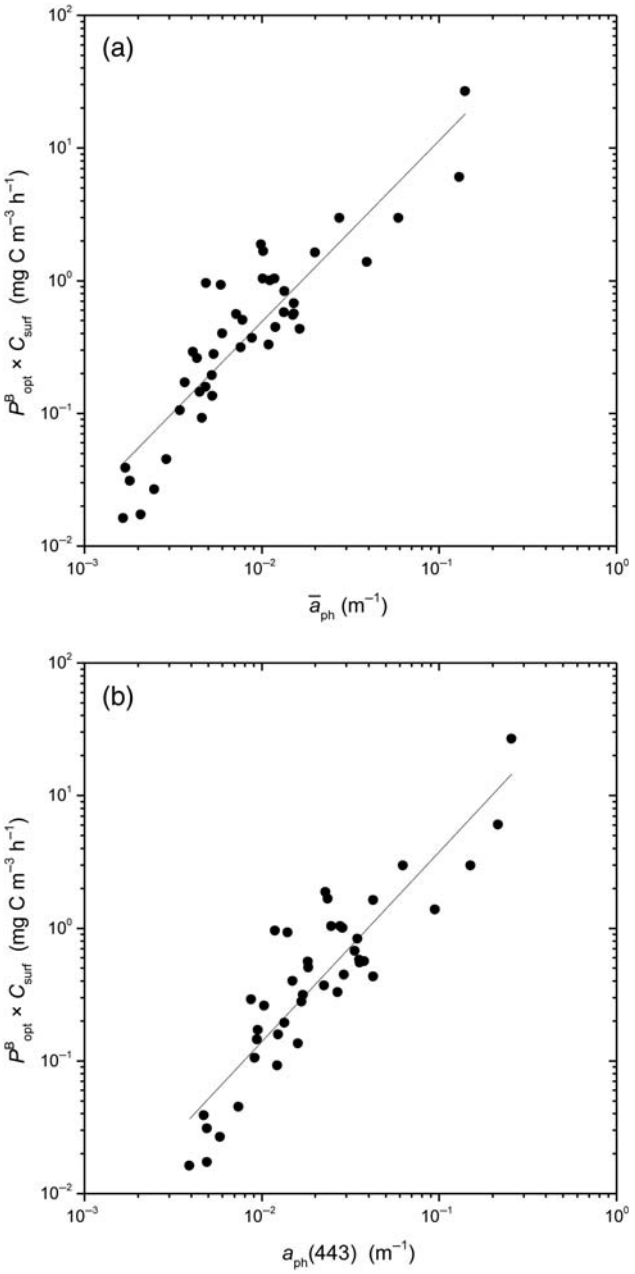

Figure 3. Relationship between *in situ* $P^B_{opt} \times C_{surf}$ and (a) the spectrally averaged light absorption coefficient of phytoplankton at the sea surface, $\bar{a}_{ph}(0-)$, from QFT data, and (b) the surface light absorption coefficient at 443 nm, $a_{ph}(443)$, from QFT data.

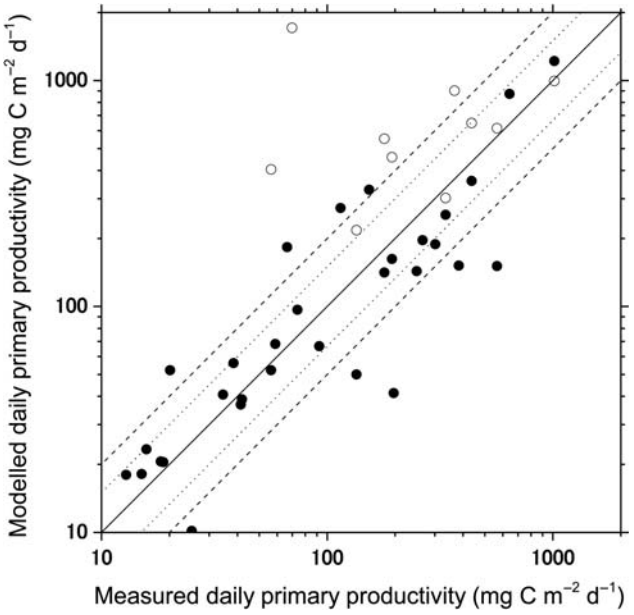

Figure 4. Comparison between measured and modelled daily primary productivity. Modelled data represented by solid circles were derived using *in situ* $R_{rs}(\lambda)$ determined by a spectroradiometer plus *in situ* PAR, and data represented by open circles were derived from MODIS $R_{rs}(\lambda)$.The solid line represents 1:1 agreement, and dashed and dotted lines represent factors of 2 and 1.5 relative errors.

Estimated daily primary productivity using the ABPM (Figure 5a) represents quite different features from the result using the VGPM (Figure 5b). The level of primary productivity obtained using the new approach is less than half that of the VGPM estimation. Extremely high productivity was not widely distributed around the coastal region of Alaska in the ABPM estimation (Figure 5a). Although the primary productivity of $>10\,000$ mg C m^{-2} d^{-1} was frequently found in the VGPM, productivity >1500 mg C m^{-2} d^{-1} using the new model was found only at the Yukon River mouth, and in the Kotzebue and Mackenzie River estuaries, where an effect of high CDOM and NAP was likely to remain because the *in situ* spectroradiometer and the QFT data used to validate $a_{ph}(443, 0-)$ were not collected in these very high CDOM and NAP regions.

The large difference in the PP_{eu} estimations between the ABPM (Figure 5a) and the VGPM (Figure 5b) might be caused by the overestimation of the Chl *a* concentration attributed to high absorption by CDOM and NAP at the blue wavelengths. To investigate the effect of CDOM and NAP on the differences in the PP_{eu} estimations, the relative difference between the two models (VGPM/ABPM; Figure 5c) was compared with the relative abundance of absorption by CDOM and NAP to phytoplankton absorption at 443 nm [$a_{dg}(443, 0-)/a_{ph}(443, 0-)$; Figure 5d]. The relationship $a_{dg}(443, 0-)/a_{ph}(443, 0-)$ was used as an index of interference by CDOM and NAP absorptions. The VGPM estimation was 1.5−5 times larger than ABPM retrieval (Figure 5c), and overall, the high VGPM/ABPM region corresponded to a high $a_{dg}(443, 0-)/a_{ph}(443, 0-)$. Note that the Russian side of the Bering Strait and western Bering Sea (55–60°N, 170°E–180°) had relatively low $a_{dg}(443, 0-)/a_{ph}(443, 0-)$ and VGPM/ABPM. Although the Chukchi Shelf region had higher values of $a_{dg}(443, 0-)/a_{ph}(443, 0-)$ of >4.0, the VGPM/ABPM ratio was ~2.5–3.5 and not as high as the coastal region of the Bering Sea.

Interannual variation in primary productivity

Interannual variation in PP_{eu} between 2002 and 2010 derived from satellite data is shown in Figure 6. The PP_{eu} derived using the new approach (Figure 6a and b) increased significantly over the 9-year period in all categories in both August ($r^2 = 0.65–0.85$, $p < 0.01$) and September ($r^2 = 0.74–0.79$, $p < 0.005$). The increments of PP_{eu} from 2006 to 2007 in the Bering Strait and over the Chukchi Shelf increased by a factor of 1.51–1.80 in August and 1.66–2.46 in September. In addition, productivity for 2006–

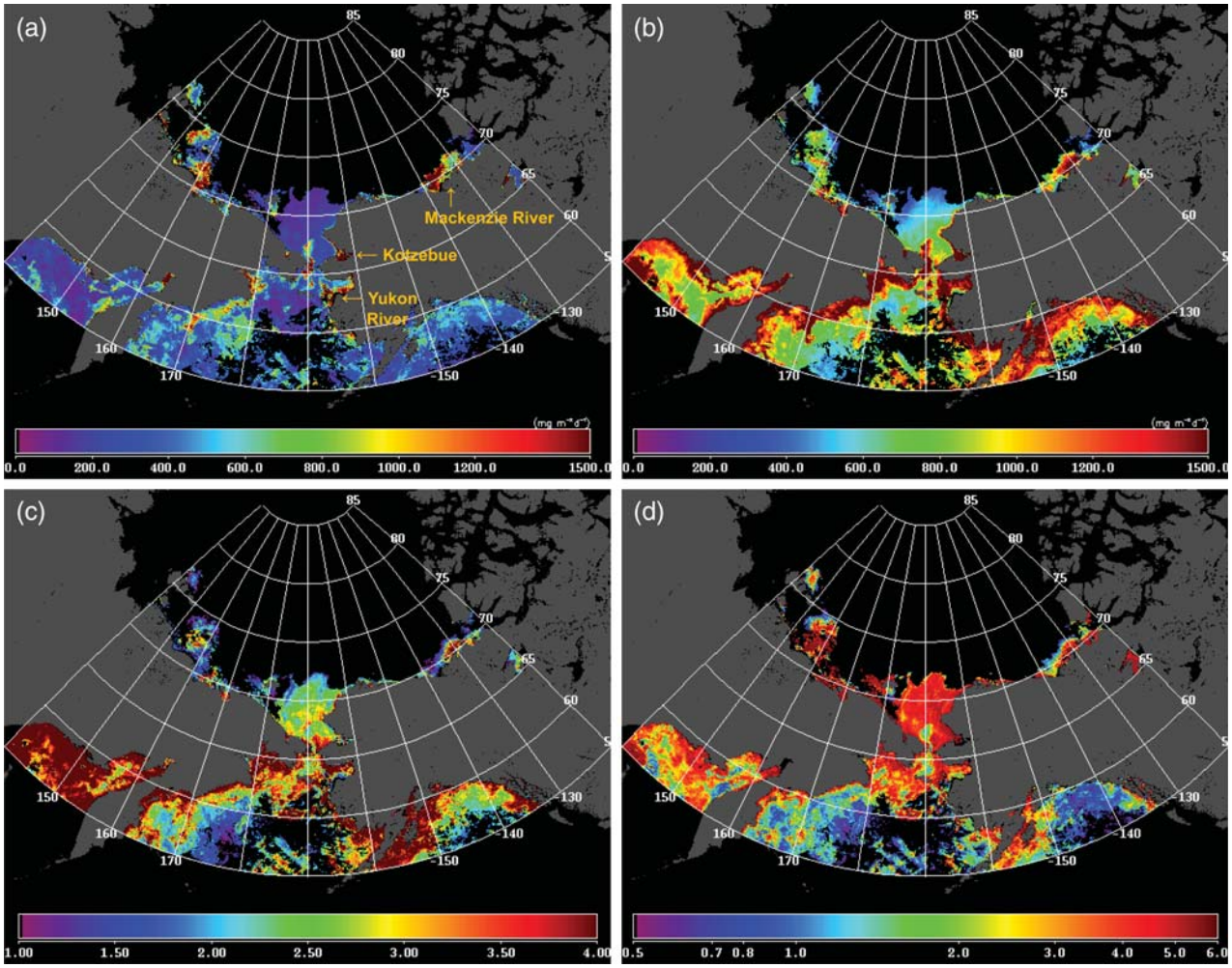

Figure 5. Distribution of daily primary productivity (PP_{eu}; mgC m^{-2} d^{-1}) from MODIS data for the Bering and Chukchi Seas. For July 2002, estimation using (a) the absorption-based productivity model (ABPM, this study) and (b) the VGPM. The ratio of the VGPM estimation to the ABPM estimation is shown in (c). The ratio of the absorption coefficient of CDOM + NAP, $a_{dg}(443)$, to that of phytoplankton, $a_{ph}(443)$, in July 2001 is shown in (d).

2007 increased by 2.71 times in September at the shelf break. Peaks of primary productivity were found in 2009 and 2010, and the value in the Bering Strait reached 983.9 mg C m^{-2} d^{-1}.

These trends are quite different from the results of the VGPM (Figure 6c and d). Productivity estimated by the VGPM in the northern Bering Sea, Bering Strait, and Chukchi shelf had a higher range, from 500 to 1900 mg C m^{-2} d^{-1}, an increasing trend was not found, and productivity in the northern Bering Sea declined in August.

Discussion

The new primary productivity model using a phytoplankton absorption coefficient developed in this study reduced the effect of CDOM in the estimation of Arctic productivity. The reliability of absorption estimation from *in situ* remote sensing reflectance data was also confirmed (Figure 2). Using the new model, an increasing trend in primary productivity during August and September of 2002–2010 was revealed.

For the phytoplankton absorption coefficient retrieved from satellite R_{rs} data, error (negative a_{ph}) is probably attributable to technical issues, such as poor accuracy in the estimation of reflectance. Several algorithms to estimate absorption coefficients other than the QAA have been developed (e.g. Garver and Siegel, 1997; Maritorena *et al.*, 2002; Smyth *et al.*, 2006), and their satellite products or source code are available from NASA. The absorption-based model in this study determines the surface production ($P^{B}_{opt} \times C_{surf}$) using the phytoplankton absorption coefficient $\bar{a}_{ph}(0-)$ or $a_{ph}(443)$ as a variable, and eliminates the dependence on Chl *a* concentration. Therefore, a function of Chl *a*, a constant value of Chl *a*-specific $a_{ph}(\lambda)$, and a fixed spectral shape of $a_{ph}(\lambda)$ should not be included in the algorithm to derive $a_{ph}(\lambda)$ for the ABPM. The QAA is a suitable algorithm for this purpose.

If $a_{ph}(412)$ of the MODIS data does not show frequent negative values, it is possible to use a spectrally averaged absorption coefficient $\bar{a}_{ph}(0-)$, as demonstrated for the Southern Ocean (Hirawake *et al.*, 2011). Using $a_{ph}(443)$ rather than $\bar{a}_{ph}(0-)$ is not only the peak of Chl *a*, but the absorption bands of other photosynthetic and accessory pigments (Bricaud and Stramski, 1990). Hence, $a_{ph}(443)$ adequately represents the absorbed light over the visible region. Indeed, Isada *et al.* (2010) obtained a significant relationship between $a_{ph}(443)$ and surface productivity in the Oyashio

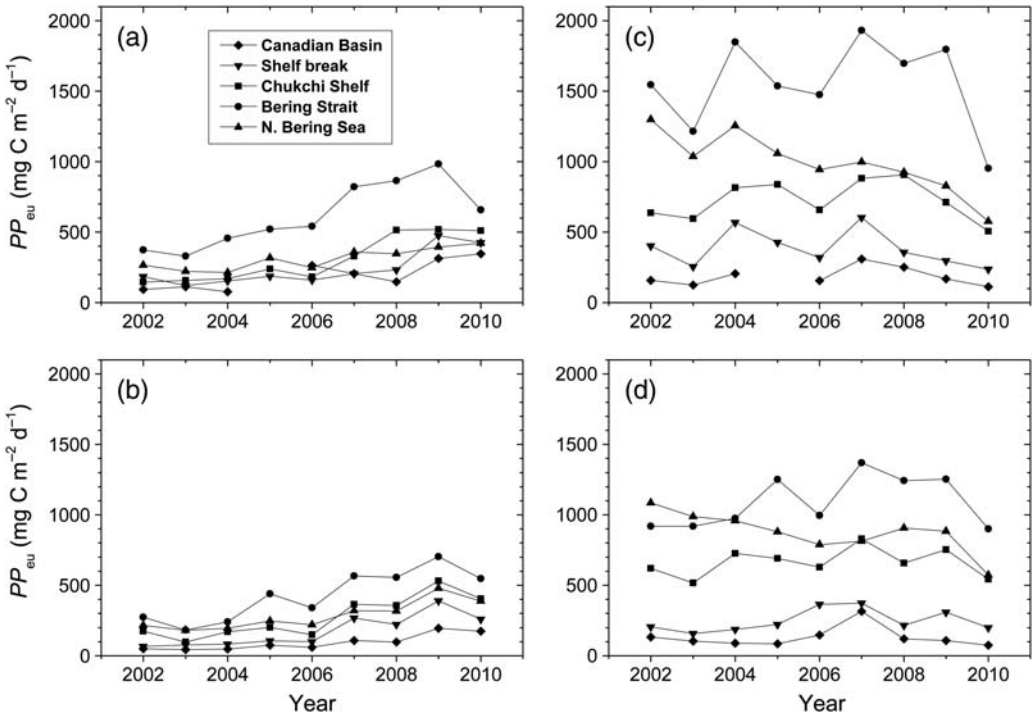

Figure 6. Interannual variation of column-integrated daily primary productivity (PP_{eu}) from 2002 to 2010 in the northern Bering Sea, the Bering Strait, the Chukchi shelf, the shelf break, and the Canada Basin. Monthly averaged data during (a) August and (b) September were input into the absorption-based productivity model (ABPM, this study). (c and d) Results for August and September using the VGPM.

region during the spring bloom, and suggested that this as a potential absorption property to apply to a primary productivity model for satellite imagery. Hirata *et al.* (2009) also utilized $a_{ph}(443)$ for estimating surface productivity in several upwelling regions and investigated the primary productivity of each dominant size class of phytoplankton.

The range of *in situ* daily primary productivity used for development of the ABPM in this study (Table 1) was generally the same as that of historical values (Springer and McRoy, 1993; Hill and Cota, 2005; Lee and Whitledge, 2005; Lee *et al.*, 2007a), as listed in Table 2. These earlier studies also reported extremely high productivity of >3000 mg C m^{-2} d^{-1} and occasionally even up to 8000 mg C m^{-2} d^{-1} (Table 2). However, waters next to the massively productive stations with >3000 mg C m^{-2} d^{-1} (Hill and Cota, 2005) showed similar productivity to this study. Although collection of a dataset including elevated productivity, such as that of a spring bloom, is desirable for model development, it is not certain whether current operational ocean colour sensors distinguish the massive blooms on an extremely small spatial scale (<1 km). As a linear relationship between surface productivity and the light absorption coefficient up to higher productivity in bloom regions has also been reported (Marra *et al.*, 2007), the model in this study is expected to detect an elevated bloom over a larger spatial scale than the spatial resolution of satellite sensors allows.

Estimated daily primary productivity using the ABPM gave a value of less than half the result using the VGPM (Figures 5 and 6). However, the values shown in Figure 5a (July 2002) coincided with the *in situ* data in the same month (Hill and Cota, 2005), which reported 783 mg C m^{-2} d^{-1} of the mean productivity over the Chukchi shelf and its shelf-break region, and 324 mg C m^{-2} d^{-1} in the Canada Basin (Table 2). Therefore, it is suggested that the VGPM overestimated the PP_{eu}. Figure 5c and d indicates that the overestimation of PP_{eu} by the VGPM can probably be attributed to an overestimation of Chl *a* concentration by contamination from a high concentration of CDOM and NAP absorptions. It is still difficult to express the effects of the CDOM and NAP absorptions on PP_{eu} estimations from the distribution maps (Figure 5c and d) because of the regional differences in the relationship between the two factors. To show the effect of $a_{dg}(443, 0-)$ on the PP_{eu} estimations, and the difference between the VGPM and ABPM more quantitatively, relationships between VGPM/ABPM and $a_{dg}(443, 0-)/a_{ph}(443, 0-)$ were expressed with a density plot (Figure 7). Overall, 90% of the values in Figure 5a and b were plotted in Figure 7 against the frequency (number of pixels). The difference between the VGPM and ABPM increased as the contribution of $a_{dg}(443, 0-)$ increased. Two trends indicating regional differences were also evident in this plot; the $\log_{10}$(VGPM/ABPM) is $\sim$0.0 (the VGPM and ABPM values are equivalent) and 0.3 (VGPM double that of ABPM) when the contribution of $a_{dg}(443, 0-)$ is half that of $a_{ph}(443, 0-)$. As shown in Figure 4, the ABPM can derive primary productivity within a factor of 2 (RMSE = 0.268). Increasing trends in the VGPM/ABPM ratio as $a_{dg}(443, 0-)/a_{ph}(443, 0-)$ rises suggest that CDOM and NAP are the main factors causing overestimation in the VGPM estimation and that the ABPM has the advantage of reducing the effect of high CDOM and NAP contribution to the optical properties of waters in the Bering and Chukchi Seas.

An increase in annual primary production attributed to an increase in open-water area in the Arctic Ocean has been reported (Pabi *et al.*, 2008; Arrigo and van Dijken, 2011). The results in

Table 2. Historical values of column-integrated daily primary productivity in the Bering and Chukchi Seas.

Area	Month and year	Method	Productivity (mg C m^2 d^{-1})	Mean productivity (mg C m^2 d^{-1})	Source
Northeastern Chukchi	July–August 1987	^{14}C	<4 700		Springer and McRoy (1993)
Chukchi shelf and shelf break	May–June 2002	^{14}C	<300	164	Hill and Cota (2005)
Canada Basin	May–June 2002			110	
Barrow Canyon	May–June 2002		8 000		
Chukchi shelf and shelf break	July–August 2002		80–2 900	783	
Canada Basin	July–August 2002			324	
Canada Basin	August–September 2002	^{13}C	79–144	109	Lee and Whitledge (2005)
Bering Strait	June 2002	^{13}C	1 428		Lee *et al.* (2007a)
Chukchi shelf	June 2002		524		
Bering Strait	July 2003		2 141		
Chukchi shelf	July 2003		765		
Bering Strait	August 2004		98–765	357	
Chukchi shelf	August 2004		72–3 578	1 100	
Northeastern Chukchi	August–September 2004		45–432	162	

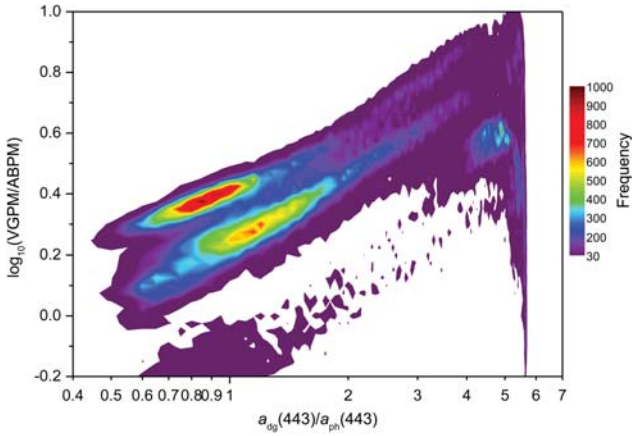

Figure 7. Density plot of log-difference between the VGPM and ABPM vs. the ratio of the absorption coefficient of CDOM + NAP, $a_{dg}(443)$, and that of phytoplankton, $a_{ph}(443)$, in July 2001. The colour scale represents the frequency (the number of pixels) in Figure 5c and d.

this study revealed that daily primary productivity also increased during the period from 2002 to 2010. Higher water temperatures were found in the Chukchi Sea in summer (Mizobata *et al.*, 2010), along with an increase in temperature-induced higher phytoplankton activity. A decrease in sea-ice extent in September led to an increase in the period of open water, so giving phytoplankton the opportunity to continue photosynthesis when nutrients were resuspended by cooling in autumn. This is especially relevant to nutrient-limited phytoplankton at the sea surface (Lee and Whitledge, 2005). These recent changes are thought to be some of the factors enhancing primary productivity during August and September. Over longer time-scales, such as a comparison with the 1970s–1990s, a decrease in primary productivity in the Bering and Chukchi Seas has been suggested (Lee *et al.*, 2007a, 2012). Lee *et al.* (2012) also doubted the increasing trend detected using satellite remote sensing (Pabi *et al.*, 2008), because of the general overestimation of Chl *a* concentrations. Our results do not explain the relationship with open-water area, but an increase in annual production is supported because the new model omitted the effect of CDOM leading to the overestimation of Chl *a* and did not use the Chl *a* parameter.

Further careful analysis and validation of the MODIS data combined with *in situ* data such as nutrients and temperature are required to confirm the trends in primary productivity calculated here. However, the ABPM in this study was a more effective tool than the Chl *a*-based one when used in the Arctic Ocean, and will likely contribute to better understanding of the response of phytoplankton to massive environmental change.

Acknowledgements

We thank T. Kikuchi and S. Nishino for their assistance, and the captains and crews of the TS "Oshoro-Maru" and RV "Mirai" for their support during the cruises. We also thank A. Tsuda for his loan of the spectroradiometer, and K. Suzuki, A. Shiomoto, and H. Kasai for their assistance in pigment and ^{13}C analysis. The research was supported in part by JSPS (KAKENHI 19405002), IARC-JAXA, and the JAXA GCOM-C programme.

References

Alexander, V., and Niebauer, H. J. 1981. Oceanography of the eastern Bering Sea ice-edge zone in spring. Limnology and Oceanography, 26: 1111–1125.

Arrigo, K. R., van Dijken, G., and Pabi, S. 2008. Impact of a shrinking Arctic ice cover on marine primary production. Geophysical Research Letters, 35: L19603.

Arrigo, K. R., and van Dijken, G. L. 2011. Secular trends in Arctic Ocean net primary production. Journal of Geophysical Research, 116: C09011.

Austin, R. W. 1974. The remote sensing of spectral radiance from below the ocean surface. *In* Optical Aspects of Oceanography, pp. 317–344. Ed. by N. G. Jerlov, and E. S. Nielsen. Academic Press, London.

Behrenfeld, M. J., and Falkowski, P. G. 1997. Photosynthetic rates derived from satellite-based chlorophyll concentration. Limnology and Oceanography, 42: 1–20.

Boé, J., Hall, A., and Qu, X. 2009. September sea-ice cover in the Arctic Ocean projected to vanish by 2100. Nature Geoscience, 2: 341–343.

Bricaud, A., and Stramski, D. 1990. Spectral absorption coefficients of living phytoplankton and nonalgal biogenous matter: a comparison between the Peru upwelling area and the Sargasso Sea. Limnology and Oceanography, 35: 562–582.

Campbell, J., Antoine, D., Armstrong, R., Arrigo, K., Balch, W., Barber, R., and Behrenfeld, M. *et al.* 2002. Comparison of algorithms for estimating ocean primary production from surface chlorophyll, temperature, and irradiance. Global Biogeochemical Cycles, 16: 1035, doi:10.1029/2001GB001444.

Comiso, J. C. 2006. Abrupt decline in the Arctic winter sea ice cover. Geophysical Research Letters, 33: L18504.

Cota, G. F., Wang, J., and Comiso, J. C. 2004. Transformation of global satellite chlorophyll retrievals with a regionally tuned algorithm. Remote Sensing of the Environment, 90: 373–377.

Feder, H. M., Jewett, S. C., and Blanchard, A. 2005. Southeastern Chukchi Sea (Alaska) epibenthos. Polar Biology, 28: 402–421.

Garver, S. A., and Siegel, D. A. 1997. Inherent optical property inversion of ocean color spectra and its biogeochemical interpretation. 1. Time series from the Sargasso Sea. Journal of Geophysical Research, 102: 18607–18625.

Gordon, H. R., Brown, O. B., Evans, R. H., Brown, J. W., Smith, R. C., Baker, K. S., and Clark, D. K. 1988. A semianalytic radiance model of ocean color. Journal of Geophysical Research, 93: 10909–10924.

Gordon, H. R., Clark, D. K., Brown, J. W., Brown, O. B., Evans, R. H., and Broenkow, W. W. 1983. Phytoplankton pigment concentrations in the Middle Atlantic Bight: comparison of ship determinations and CZCS estimates. Applied Optics, 22: 20–36.

Grebmeier, J. M., Cooper, L. W., Feder, H. M., and Sirenko, B. I. 2006a. Ecosystem dynamics of the Pacific-influenced northern Bering and Chukchi Seas in the Amerasian Arctic. Progress in Oceanography, 71: 331–361.

Grebmeier, J. M., McRoy, C. P., and Feder, H. M. 1988. Pelagic-benthic coupling on the shelf of the northern Bering and Chukchi Seas. 1. Food-supply source and benthic biomass. Marine Ecology Progress Series, 48: 57–67.

Grebmeier, J. M., Overland, J. E., Moore, S. E., Farley, E. V., Carmack, E. C., Cooper, L. W., and Frey, K. E. *et al.* 2006b. A major ecosystem shift in the northern Bering Sea. Science, 311: 1461–1464.

Guéguen, C., Guo, L., Yamamoto-Kawai, M., and Tanaka, N. 2007. Colored dissolved organic matter dynamics across the shelf-basin interface in the western Arctic Ocean. Journal of Geophysical Research, 112: C05038.

Hama, T., Miyazaki, T., Ogawa, Y., Iwakuma, T., Takahashi, M., Otsuki, A., and Ichimura, S. 1983. Measurement of photosynthetic production of a marine phytoplankton population using a stable ^{13}C isotope. Marine Biology, 73: 31–36.

Hill, V., and Cota, G. 2005. Spatial patterns of primary production on the shelf, slope and basin of the western Arctic in 2002. Deep Sea Research II, 52: 3344–3354.

Hill, V. J., and Zimmerman, R. C. 2010. Estimates of primary production by remote sensing in the Arctic Ocean: assessment of accuracy with passive and active sensors. Deep Sea Research I, 57: 1243–1254.

Hirata, T., Hardman-Mountford, N. J., Barlow, R., Lamont, T., Brewin, R., Smyth, T., and Aiken, J. 2009. An inherent optical property approach to the estimation of size-specific photosynthetic rates in eastern boundary upwelling zones from satellite ocean colour: an initial assessment. Progress in Oceanography, 83: 393–397.

Hirawake, T., Takao, S., Horimoto, N., Ishimaru, T., Yamaguchi, Y., and Fukuchi, M. 2011. A phytoplankton absorption-based primary productivity model for remote sensing in the Southern Ocean. Polar Biology, 34: 291–302.

Holland, M., Serreze, M., and Stroeve, J. 2010. The sea ice mass budget of the Arctic and its future change as simulated by coupled climate models. Climate Dynamics, 34: 185–200.

Isada, T., Hattori-Saito, A., Saito, H., Ikeda, T., and Suzuki, K. 2010. Primary productivity and its bio-optical modeling in the Oyashio region, NW Pacific during the spring bloom 2007. Deep Sea Research II, 57: 1653–1664.

Kishino, M., Takahashi, M., Okami, N., and Ichimura, S. 1985. Estimation of the spectral absorption coefficients of phytoplankton in the sea. Bulletin of Marine Science, 37: 634–642.

Lee, S. H., Joo, H. M., Yun, M. S., and Whitledge, T. E. 2012. Recent phytoplankton productivity of the northern Bering Sea during early summer in 2007. Polar Biology, 35: 83–98.

Lee, S. H., and Whitledge, T. E. 2005. Primary and new production in the deep Canada Basin during summer 2002. Polar Biology, 28: 190–197.

Lee, S. H., Whitledge, T. E., and Kang, S. H. 2007a. Recent carbon and nitrogen uptake rates of phytoplankton in Bering Strait and Chukchi Sea. Continental Shelf Research, 27: 2231–2249.

Lee, Z. P., Carder, K. L., and Arnone, R. A. 2002. Deriving inherent optical properties from water color: a multiband quasi-analytical algorithm for optically deep waters. Applied Optics, 41: 5755–5772.

Lee, Z. P., Weidemann, A., Kindle, J., Arnone, R., Carder, K. L., and Davis, C. 2007b. Euphotic zone depth: its derivation and implication to ocean-color remote sensing. Journal of Geophysical Research, 112: C03009.

Maritorena, S., Siegel, D. A., and Peterson, A. R. 2002. Optimization of a semianalytical ocean color model for global-scale applications. Applied Optics, 41: 2705–2714.

Marra, J., Trees, C. C., and O'Reilly, J. E. 2007. Phytoplankton pigment absorption: a strong predictor of primary productivity in the surface ocean. Deep Sea Research I, 54: 155–163.

Matsuoka, A., Hill, V., Huot, Y., Babin, M., and Bricaud, A. 2011. Seasonal variability in the light absorption properties of western Arctic waters: parameterization of the individual components of absorption for ocean color applications. Journal of Geophysical Research, 116: C02007.

Matsuoka, A., Huot, Y., Shimada, K., Saitoh, S. I., and Babin, M. 2007. Bio-optical characteristics of the western Arctic Ocean: implications for ocean color algorithms. Canadian Journal of Remote Sensing, 33: 503–518.

Mitchell, B. G. 1990. Algorithms for determining the absorption coefficient of aquatic particulates using the quantitative filter technique (QFT). *In* Ocean Optics X, pp. 137–148. Ed. by R. W. Spinrad. Proceedings of the SPIE, 1302.

Mizobata, K., Shimada, K., Woodgate, R., Saitoh, S., and Wang, J. 2010. Estimation of heat flux through the eastern Bering Strait. Journal of Oceanography, 66: 405–424.

Moore, S. E., Grebmeier, J. M., and Davies, J. R. 2003. Gray whale distribution relative to forage habitat in the northern Bering Sea: current conditions and retrospective summary. Canadian Journal of Zoology, 81: 734–742.

Morel, A., and Maritorena, S. 2001. Bio-optical properties of oceanic waters: a reappraisal. Journal of Geophysical Research, 106: 7163–7180.

Neckel, H., and Labs, D. 1984. The solar radiation between 3300 and 12500 A. Solar Physics, 90: 205–258.

Pabi, S., van Dijken, G. L., and Arrigo, K. R. 2008. Primary production in the Arctic Ocean, 1998–2006. Journal of Geophysical Research, 113: C08005.

Parkinson, C. L., and Cavalieri, D. J. 2008. Arctic sea ice variability and trends, 1979–2006. Journal of Geophysical Research, 113: C07003.

Piepenburg, D. 2005. Recent research on Arctic benthos: common notions need to be revised. Polar Biology, 28: 733–755.

Shimada, K., Kamoshida, T., Itoh, M., Nishino, S., Carmack, E., McLaughlin, F., and Zimmermann, S. *et al.* 2006. Pacific Ocean inflow: influence on catastrophic reduction of sea ice cover in the Arctic Ocean. Geophysical Research Letters, 33: L08605.

Smyth, T. J., Moore, G. F., Hirata, T., and Aiken, J. 2006. Semianalytical model for the derivation of ocean color inherent

optical properties: description, implementation, and performance assessment. Applied Optics, 45: 8116–8131.

Springer, A. M., and McRoy, C. P. 1993. The paradox of pelagic food webs in the northern Bering Sea. 3. Patterns of primary production. Continental Shelf Research, 13: 575–599.

Suzuki, K., Hinuma, A., Saito, H., Kiyosawa, H., Liu, H., Saino, T., and Tsuda, A. 2005. Responses of phytoplankton and heterotrophic bacteria in the northwest subarctic Pacific to *in situ* iron fertilization as estimated by HPLC pigment analysis and flow cytometry. Progress in Oceanography, 64: 167–187.

Suzuki, R., and Ishimaru, T. 1990. An improved method for the determination of phytoplankton chlorophyll using N, N-Dimethylformamide. Journal of the Oceanographical Society of Japan, 46: 190–194.

van Heukelem, L., and Thomas, C. S. 2001. Computer-assisted high-performance liquid chromatography method development with applications to the isolation and analysis of phytoplankton pigments. Journal of Chromatography A, 910: 31–49.

Welschmeyer, N. A. 1994. Fluorometric analysis of chlorophyll *a* in the presence of chlorophyll *b* and pheopigments. Limnology and Oceanography, 39: 1985–1992.

Woodgate, R. A., Weingartner, T., and Lindsay, R. 2010. The 2007 Bering Strait oceanic heat flux and anomalous Arctic sea-ice retreat. Geophysical Research Letters, 37: L01602.

Handling editor: Audrey Geffen